RESEARCH ARTICLE | SEPTEMBER 20 2017

All-Si photodetector for telecommunication wavelength based on subwavelength grating structure and critical coupling

Alireza Taghizadeh ; Aref Rasoulzadeh Zali; Il-Sug Chung; Mohammad Kazem Moravvej-Farshi

AIP Advances 7, 095019 (2017)
https://doi.org/10.1063/1.4995700

All-Si photodetector for telecommunication wavelength based on subwavelength grating structure and critical coupling

Alireza Taghizadeh,[1,2,a] Aref Rasoulzadeh Zali,[1,3,b] Il-Sug Chung,[1] and Mohammad Kazem Moravvej-Farshi[3]
[1]*Department of Photonics Engineering (DTU Fotonik), Technical University of Denmark, DK-2800 Kgs. Lyngby, Denmark*
[2]*Department of Physics and Nanotechnology, Aalborg University, DK-9220 Aalborg East, Denmark*
[3]*Faculty of Electrical and Computer Engineering, Advanced Devices Simulation Lab (ADSL), Tarbiat Modares University, PO Box 14115-194, Tehran 1411713116, Iran*

(Received 12 January 2017; accepted 13 September 2017; published online 20 September 2017)

We propose an efficient planar all-Si internal photoemission photodetector operating at the telecommunication wavelength of 1550 nm and numerically investigate its optical and electrical properties. The proposed polarization-sensitive detector is composed of an appropriately engineered subwavelength grating structure topped with a silicide layer of nanometers thickness as an absorbing material. It is shown that a nearly-perfect light absorption is possible for the thin silicide layer by its integration to the grating resonator. The absorption is shown to be maximized when the critical coupling condition is satisfied. Simulations show that the external quantum efficiency of the proposed photodetector with a 2-nm-thick PtSi absorbing layer at the center wavelength of 1550 nm can reach up to ~60%. https://doi.org/10.1063/1.4995700

Silicon (Si) photonics have been considered as a promising pathway to realize low-cost integration of photonic devices with electronics, particularly for optical communication applications, thanks to the complementary metal-oxide-semiconductor (CMOS) compatibility.[1] In optical communication systems, a photodetector (PD) is an essential building block device, and for Si photonics it needs to be integrated into a Si wafer by using CMOS-compatible processes. Although Si-based PDs have been widely used for visible light wavelength range (0.4 to 0.7 μm), they can not be simply employed for communication wavelength range (1.3 to 1.6 μm), since the photon's energy in the communication wavelengths is smaller than Si bandgap energy E_g of 1.1 eV. Several approaches have been suggested for making a Si-based PD in the communication wavelength range, including hybrid integration of either III-V materials or Ge into Si using a wafer-bonding technique,[2–4] growth of Ge on Si,[5,6] and the use of internal photoemission effect (IPE) based on a Schottky barrier.[7–11] In the last approach, employing a metallic silicide layer with nanometer thickness adjacent to Si forms a Schottky barrier of height ϕ_B at the metal-Si interface. At this interface, the photons with energy $h\nu$ (h and ν are the Planck constant and photon frequency) in the range of $\phi_B < h\nu < E_g$ are absorbed in the silicide layer and can overcome the Schottky barrier ϕ_B, being collected at an external contact connected to the Si layer.

For PDs, one of the most important specifications is the external quantum efficiency η_e, which is given by $\eta_e = A\eta_i$. Here, the optical absorption efficiency A measures the ratio of incident photons turning into photo-carriers in the absorbing layer and the internal quantum efficiency (IQE) η_i measures the ratio of the photo-carriers arriving at an external contact.[9] Thus, for achieving a high

[a]Corresponding author: alitag@fotonik.dtu.dk
[b]The first and second authors have contributed equally to this work.

external quantum efficiency, both the absorption and the IQE should be maximized. For an IPE-based PD, the IQE can be enhanced by thinning down the silicide layer far below the carriers mean free path.[7,12] This makes more photo-carriers arriving at the Si layer before being scattered in the silicide layer.[10,13] However, this approach may lead to a significant reduction in the optical absorption efficiency. To enhance the optical absorption efficiency as well as the IQE, one can integrate the IPE-PD into a resonator structure such as a microring resonator[14] or a Fabry-Perot cavity.[15]

To tackle these challenges, here we propose a CMOS-compatible PD structure, based on the Schottky-barrier IPE and a recently-suggested subwavelength grating resonator. As illustrated schematically in Fig. 1(a), the proposed PD structure consists of a silicide layer, a p-doped Si layer referred to as the *cap layer*, and a Si grating layer. The cap layer and grating layer form a *hybrid grating* (HG) resonator, which allows for almost complete absorption as shown below. The HG is a variant of the high-contrast grating (HCG)[16–18] and has an un-patterned cap layer on top of a near-subwavelength grating layer.[19–21] It has been shown that HGs can provide extraordinary properties including high quality-factors ($Q>10^7$)[19] and high reflectivity (>99%) over a broad bandwidth.[20] As an important feature, HG-based lasers and photodetectors facilitate the fabrication process compared to HCG-based ones.[4,19] Although the HG is usually comprised of two different materials such as Si for the grating and InP for the cap layer,[4,19,20] both the grating and cap layer are made of the same material (Si) in this work. Furthermore, the unit-cell of grating is engineered in order to obtain 100% absorption at the desired wavelength. Since the HG properties depend on the light polarization,[19,20] the proposed PD can detect the light with a specific polarization, which may be useful for communication applications. Moreover, by employing a two-dimensional grating structure,[22] a polarization-insensitive PD can be designed similarly. In our earlier work,[10] we have proposed an IPE-based PD structure using a microring resonator. This structure requires deposition of a silicide layer on a selected part of ring sidewall, which is not a feasible process. The proposed structure of this work does not require this non-planar process and is more compact. Furthermore, the light can easily be coupled to the suggested PD from the free space in the surface-normal direction, which is challenging for the microring structure and requires extra effort.

The rest of paper is organized as follows. First, the proposed PD structure is presented. Then, a brief review of the model used to calculate the IQE is discussed, and IQEs of several types of silicide layers are compared. Then, the optical simulation method is briefly explained and the working mechanism for achieving perfect absorption by employing subwavelength grating structure is explained. Numerical simulation of absorption illustrates that the critical coupling condition is satisfied for the chosen thickness of the silicide layer. Finally, the paper is closed by the conclusion.

Figure 1(a) shows a schematic of the proposed PD structure. When fabricating this structure, a grating is firstly formed in the Si layer of a silicon-on-insulator (SOI) wafer using E-beam lithography. Then, another SOI wafer with a p-doped Si layer (e.g., 10^{17} cm^{-3} doping concentration) is wafer-bonded to the grating layer, and the Si substrate and buried oxide layer of the wafer-bonded SOI wafer are removed, leaving the p-doped Si as the cap layer. A thin layer of silicide with a thickness

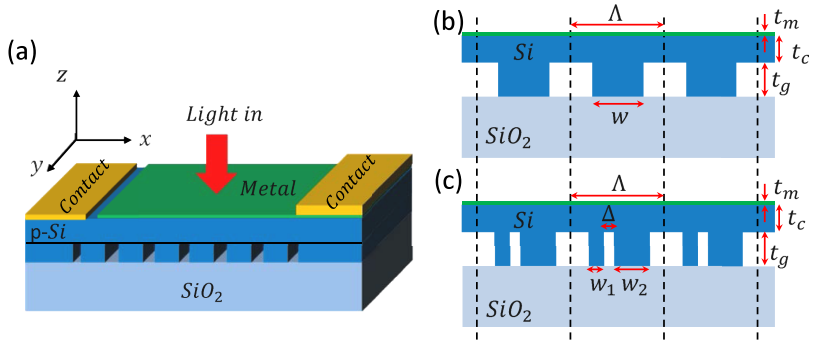

FIG. 1. (a) Schematic view of the proposed photodetector structure, which consists of a Si grating layer (blue color) on a SiO_2 substrate, a Si cap layer (blue-color p-doped Si), and a thin silicide layer (green color). (b),(c) Schematic cross-sectional view of the device in the *xz*-plane with parameter symbol definitions. In (c) the unit-cell of the grating is engineered.

of t_m is deposited on top of the p-doped Si cap layer. Finally, ohmic contacts are formed on the Si cap layer and the silicide layer, far enough from the center of device, in order to have negligible effect on the optical field inside the device. A schematic cross-sectional view of the PD is depicted in Fig. 1(b). As discussed below, the grating unit-cell can be engineered as shown in Fig. 1(c), in order to obtain perfect absorption. This shape of unit-cell has a feasible fabrication process while it breaks the in-plane symmetry of the structure, which provides an additional set of modes to be available to enhance the absorption as discussed below. Other shapes of unit-cell with more sections in each unit-cell may be also possible but they can make the fabrication more challenging and are not investigated in this work.

To evaluate the IQE of IPE based PDs, several models have been developed.[12,15,23] In this paper, we have employed the model developed in Ref. 12 to predict carriers' emission probability from silicide-nanolayer into the Si layer per incident photon of energy $h\nu$. Though, this model is rigorously valid at cryogenic temperature, it has been shown experimentally that it can predict the efficiency of the IPE-based PD at room temperature with relatively good accuracy.[24,25] Based on this model, $\eta_i = 1/h\nu \int_{\phi_B}^{h\nu} P(E)\mathrm{d}E$,[12] where $P(E)$ is the probability of carriers with the energy of E overcoming the Schottky barrier ϕ_B. According to this model, if the silicide layer thickness t_m is much smaller than the carrier scattering length l_h ($t_m \ll l_h$), the carriers experience a number of reflections from the metal boundaries.

As shown in Fig. 2(a) and 2(b), the variation of t_m and ϕ_B can greatly affect η_i and $P(E)$. For different silicide layers such as PtSi, Pd_2Si, $CoSi_2$, and $TaSi_2$, by gradually thinning down the silicide layer from $t_m = l_h$ to t_m=0.013l_h, $P(E)$ increases by approximately 4, 5.3, 5.9, and 5.9 times, respectively. This is because by decreasing the thickness of silicide layer, a number of reflections by each hot carrier from the boundaries increases and as a result the η_i is enhanced by approximately 5, 5.8, 5.7, 5.1 times, for the respective material. Thus, to maximize the η_i, t_m should be kept as thin as practically possible to increase the carrier emission probability $P(E)$. For the rest of paper, we choose PtSi as the absorbing material due to its superior IQE compared to the others, while a 2-nm-thick layer is assumed in our optical simulations which is feasible for fabrication.[9,26] Although the grating structure is designed to have maximum absorption for PtSi layer, we have redesigned the structure for a 2nm-thick Pd_2Si and $TaSi_2$ and we manage to achieve almost 100% absorption but these results are not reported here. For other thickness of metals, we believe that it should be possible to find a design by scanning the possible design space. The parameters used for our calculations are the same as in Ref. 10.

It has been well-known for a long time that the single-pass absorption efficiency of a thin absorbing layer in air (e.g. a thin metallic layer in air) can reach 50% at most.[27,28] The maximum of 50% is due to the symmetry of the field in the absorbing layer.[27,28] However, one can overcome this limit by employing the concept of coherent perfect absorption (CPA).[29] In a CPA configuration, by coherently illuminating the thin absorbing layer from both sides (using two in-phase optical beams), a perfect absorption can be achieved, which can be interpreted also as the time-reversed phenomena of lasing action.[29,30] Instead of using coherent two-sided illumination, perfect absorption can occur with a single-sided illumination simply by employing a perfect mirror, using the critical coupling

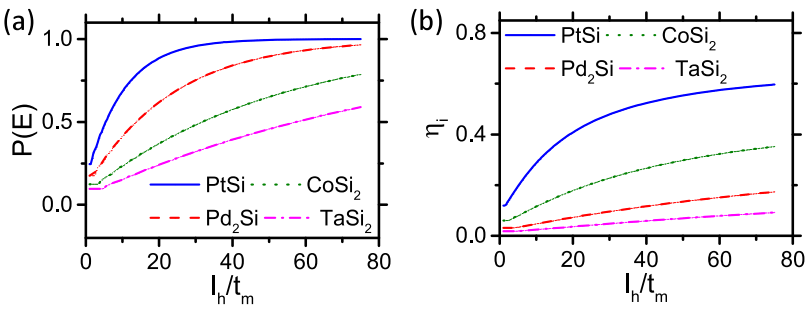

FIG. 2. (a) The PD IQE η_i, and (b) the probability by which a carrier of energy E can surmount the corresponding Schottky-barrier $P(E)$, as a function of the carrier scattering length over the silicide layer thickness l_h/t_m, for four different types of silicides; PtSi(blue), Pd_2Si(red), Co_2Si(green), and Ta_2Si(magenta).

condition. Whenever the radiative loss of a resonator is equal to its absorption loss the critical coupling condition is satisfied, which has been used widely in optics.[27,31] For instance, it has been shown that almost 100% absorption is possible in a resonant cavity enhanced PD, by appropriately designing the mirror reflectivity amplitude to satisfy the critical coupling condition.[32]

Perfect absorption is also possible for a single-side illumination without a mirror. For instance, in a symmetric photonic crystal membrane as a resonator by tuning the structure dimensions, light can be totally absorbed using degenerate critical coupling, i.e. two degenerate optical modes (have the same frequency) of opposite symmetry with respect to the reflection plane, are in critical coupled condition simultaneously.[27] More recently, it has been shown that by designing a highly asymmetric leakage rate to a substrate and a superstrate, nearly unity absorption is possible for a resonator.[33] This was performed by breaking the symmetry of a grating structure in both vertical (the light propagation direction) and transverse (the grating plane) directions. For an HG structure, the symmetry is already broken in the vertical direction. Thus, by engineering the grating unit-cell, we can achieve the total absorption. The HG structure with engineered unit-cell is more feasible for fabrication compared to the structure suggested in Ref. 33. The unit-cell of the proposed device is shown schematically in the Fig. 1(c). Each grating bar is divided in two asymmetric sections of w_1 and w_2 width, which are separated with a distance of Δ.

The numerical results for optical absorption is based on an in-house developed simulator,[21,34,35] which employs rigorous coupled wave analysis (RCWA) method[36] in combination with the scattering matrices.[37] The RCWA is also referred to as Fourier modal method (FMM). In our simulations, the grating is assumed to be infinitely periodic in the x-direction and infinitely long in the y-direction. The structure is designed for the transverse electric (TE) polarized light, i.e., electric field parallel to the grating bars. Analogously, one may achieve total absorption for transverse magnetic (TM) polarized light by changing structure dimensions. For simplicity, it is assumed that Si and SiO_2 are lossless and non-dispersive with refractive indices of 3.48 and 1.48 respectively, which is a good approximation in the wavelength range of our interest. It should be noted that the free carrier absorption of the p-doped Si at 1.55 μm wavelength is negligible (the absorption coefficient is 0.84 1/cm[38]).

In our design, we kept the ratios w_1/Λ=0.15, w_2/Λ=0.35 and Δ/Λ=0.125 constant, and varied the Λ, t_c, and t_g in the possible ranges to find a design with 100% absorption at our target wavelength of 1.55 μm. The period Λ is varied in a range, for which only 0-th diffraction order is propagating in the substrate and superstrate regions at normal incident. The values of w_i and Δ are chosen to make grating fabrication feasible while breaking the symmetry of the grating unit-cell. However, they can be chosen differently while it is still possible to obtain the perfect absorption. The reflection R, transmission T and absorption A(=1-R-T) spectra of a possible design is shown in Fig. 3(a). The absorption reaches 99.9% at wavelength of 1.55 μm, which results in external quantum efficiency and responsivity of approximately 60% and 0.75 A/W, respectively. Furthermore, the absorption is larger than 50% in a 37-nm bandwidth due to the existence of a second mode in the 1.55 μm region.

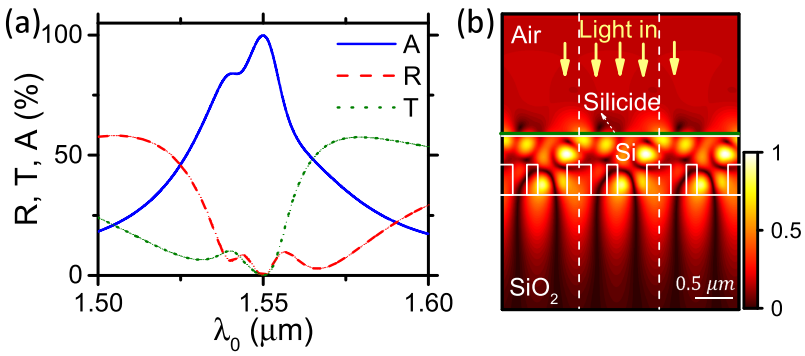

FIG. 3. (a) The absorption A(blue), reflection R(red), and transmission T(green) spectra of a designed structure excited by a normal-incident TE polarized plane-wave (in percentage). The device dimension symbols are defined in Fig. 1(c), and have values of w_1=150.8 nm, w_2=377 nm, Δ=125.7 nm, t_m=2 nm, t_c=302 nm, t_g=390 nm, and Λ=1005 nm. The absorption reaches 99.9% at 1.55 μm wavelength. (b) The normalized electric field (E_y) of the structure at 1.55 μm wavelength.

The nature of the peak in spectra is a guided-mode resonance which is well-known phenomena for the grating structures.[19,20,39] A normalized electric field profile at the total absorption wavelength is shown in Fig. 3(b).

In order to further analyze the device, we investigate the structure optical modes using the quasi-normal mode (QNM) picture as explained in Ref. 34. In the QNM picture, the optical system is viewed as an open system with only outward emission. In this work, in case that the loss in the metal is absent, there are two optical modes close to the wavelength of interest with resonance wavelengths of λ_1=1543.6 and λ_2=1554 nm and corresponding radiative Q-factor of $Q_{1,r}$=589 and $Q_{2,r}$=220. By including the loss, the resonance wavelengths barely change but their Q-factor drop to $Q_{1,t}$=145 and $Q_{2,r}$=112, respectively, which include both radiative and non-radiative losses. The non-radiative Q-factor values can be estimated using the well-known relationship of $1/Q_{i,t}=1/Q_{i,r}+1/Q_{i,nr}$, i=1,2 as $Q_{1,nr}$=192 and $Q_{1,r}$=228, respectively for two modes. For a single optical mode, using the coupled mode theory (CMT) the absorption is determined from the expression:[27]

$$A(\omega)=\frac{2\gamma_r\gamma_{nr}}{(\omega-\omega_0)^2+(\gamma_r+\gamma_{nr})^2}, \tag{1}$$

where ω_0 is the resonance wavelength and γ_r and γ_{nr} are radiative and non-radiative losses, respectively and obtained as $\gamma_r=\omega_0/Q_r$ and $\gamma_{nr}=\omega_0/Q_{nr}$. If there are two modes which are spectrally close to each other while they have negligible coupling, for instance due to the different symmetry as in Ref. 27, the total absorption can be obtained by summing up the individual absorption obtained from the above expression as shown in the Appendix. However, for the present case, this assumption breaks down due to a strong coupling between two modes. We have confirmed that the absorption peak from CMT with no inter-mode coupling will be 74% compared to the 99.7% of Fig. 3), which shows the importance of inter-mode coupling. Thus, the interference effect due to the inter-mode coupling enhances the peak absorption in this structure. Further investigation is required for modifying the CMT to include inter-mode coupling, which will be presented elsewhere.

The absorption is maximized at the critically coupled condition, which is similar to other types of resonant structures.[27,28,33] Figure 4(a) shows the absorption as the function of imaginary part of PtSi refractive index. Though, the imaginary part of material refractive index is not engineered here, and it is assumed to be a given constant at a specific wavelength, this graph can provide insight for the critically-coupled nature of the high absorption. Due to the existence of two modes and an strong coupling between them as explained above, the critical coupling process is more complex. However at $Im\{n\}$=4.25, which is the value used in the calculations of previous paragraph, the radiative and non-radiative Q-factor of two modes are approximately equal, giving rise to high absorption. It should be noted that the proposed PD structure is polarization sensitive, and the absorption for TM polarized light is less than 10% in the similar wavelength range. Although all the spectra are obtained for a normal-incident plane-wave, the absorption is angle dependent. Figure 4(b) illustrates the absorption as the function of incident angle θ at a constant wavelength of 1.55 μm. The absorption slowly decreases by increasing the angle of incidence due to the low Q-factor of the resonance. However, more than 56% absorption is still possible at 8 degree incident angle for the wavelength of 1.55 μm, which is sufficient for absorbing mostly a relatively small optical beam. It should be noted that by

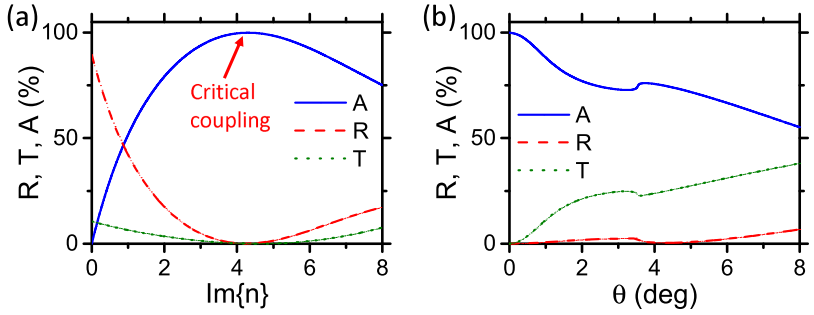

FIG. 4. (a) The absorption A(blue), reflection R(red), and transmission T(green) for the structure of Fig. 3 at the wavelength of 1.55 μm as a function of (a) imaginary part of PtSi refractive index $Im\{n\}$, and as (b) angle of incidence θ.

increasing the incident angle, the resonance wavelength of peak absorption is changed to another wavelength. This peak value drops in a much slower rate than what is plotted in Fig. 4(b).

In conclusion, we have proposed a planar, polarization-sensitive, and CMOS-compatible Si-based IPE PD with high efficiency for communication wavelength range. By embedding a thin silicide layer into a wavelength grating structure with an engineered unit-cell, a nearly-perfect absorption has been achieved when the critical coupling condition is satisfied. The external quantum efficiency of 60% is expected from theory. We believe that the proposed structure can be interesting for Si photonic applications due to its planer and feasible fabrication process.

The authors gratefully acknowledge support from the Innovation Fund Denmark through the HOT project (Grant No. 5106-00013B).

APPENDIX: CMT WITH INTERMODE COUPLING

In this section, a CMT formalism with inter-mode coupling is derived following the notation of Ref. 40. For a resonator with several optical modes and multiple external ports, the CMT is written as:

$$\frac{\mathrm{d}\,|a\rangle}{\mathrm{d}t} = (j\boldsymbol{\Omega} - \boldsymbol{\Gamma}_r - \boldsymbol{\Gamma}_{nr})\,|a\rangle + \boldsymbol{D}^T\,|s_+\rangle\,, \tag{A1a}$$

$$|s_-\rangle = \boldsymbol{C}\,|s_+\rangle + \boldsymbol{D}\,|a\rangle\,, \tag{A1b}$$

where $|s_+\rangle$, $|s_-\rangle$ and $|a\rangle$ are the vectors containing the amplitude of resonator modes, the incoming and outgoing waves, respectively, while $\boldsymbol{\Gamma}_r$ and $\boldsymbol{\Gamma}_{nr}$ are the matrices contain the radiative and non-radiative loss of the optical modes, respectively. Matrices $\boldsymbol{C}$ and $\boldsymbol{D}$ are the direct path scattering, coupling matrices, respectively, and T superscript denotes the matrix transpose operation. Due to the energy conservation, reciprocity and time-reversal symmetry, additional constrains are obtained between these matrices as:[40]

$$\boldsymbol{D}^\dagger\boldsymbol{D} = 2\boldsymbol{\Gamma}_r, \tag{A2a}$$

$$\boldsymbol{C}\boldsymbol{D}^* = -\boldsymbol{D}, \tag{A2b}$$

where $\dagger$ and $*$ superscripts denote the conjugate transpose and complex conjugate, respectively. Assuming a harmonic time dependence for the amplitudes, the system scattering matrices in the frequency domain can be obtained by relating the output $|s_-\rangle$ to the input $|s_+\rangle$ waves as:

$$\boldsymbol{X}(\omega) = j(\omega\boldsymbol{I} - \boldsymbol{\Omega}) + \boldsymbol{\Gamma}_r + \boldsymbol{\Gamma}_{nr}, \tag{A3a}$$

$$|a\rangle = \boldsymbol{X}^{-1}(\omega)\boldsymbol{D}^T\,|s_+\rangle\,, \tag{A3b}$$

$$|s_-\rangle = \boldsymbol{S}(\omega)\,|s_+\rangle = (\boldsymbol{C} + \boldsymbol{D}\boldsymbol{X}^{-1}\boldsymbol{D}^T)\,|s_+\rangle\,. \tag{A3c}$$

When the non-radiative loss is absent $\boldsymbol{S}\boldsymbol{S}^\dagger = \boldsymbol{I}$, which corresponds to the fact that system is Hermitian, i.e., no power loss in the system. If non-radiative loss presents, we can define a matrix $\boldsymbol{A} = \boldsymbol{I} - \boldsymbol{S}\boldsymbol{S}^\dagger$, for which its components show the power loss or absorption. After sum algebra, the matrix $\boldsymbol{A}$ is determined as:

$$\boldsymbol{A}(\omega) = \boldsymbol{D}[\boldsymbol{X}^{-1} + \boldsymbol{X}^{-1,\dagger} - 2\boldsymbol{X}^{-1}\boldsymbol{\Gamma}_r^*\boldsymbol{X}^{-1,\dagger}]\boldsymbol{D}^\dagger. \tag{A4a}$$

When there is no coupling between the modes, e.g. they are separated in the frequency or have different symmetry properties, all $\boldsymbol{\Omega}$, $\boldsymbol{\Gamma}_r$, $\boldsymbol{\Gamma}_{nr}$ and $\boldsymbol{X}$ are diagonal. This makes the total absorption as the sum of individual mode by using Eq. (1). However, if inter-mode coupling is non-negligible, this breaks down and an interference-type absorption may be introduced. Introducing the inter-mode coupling in CMT is not straightforward, and requires further investigation which will be presented elsewhere.

[1] B. Jalali and S. Fathpour, J. Lightwave Technol. **24**, 4600 (2006).
[2] H. Park, A. W. Fang, R. Jones, O. Cohen, O. Raday, M. N. Sysak, M. J. Paniccia, and J. E. Bowers, Opt. Express **15**, 6044 (2007).
[3] L. Chen, P. Dong, and M. Lipson, Opt. Express **16**, 11513 (2008).
[4] S. Learkthanakhachon, A. Taghizadeh, G. C. Park, K. Yvind, and I.-S. Chung, Opt. Express **24**, 16512 (2016).
[5] S. Fama, L. Colace, G. Masini, G. Assanto, and H.-C. Luan, Appl. Phys. Lett. **81**, 586 (2002).

[6] J. Michel, J. Liu, and L. C. Kimerling, Nat. Photon. **4**, 527 (2010).
[7] M. Casalino, L. Sirleto, L. Moretti, and I. Rendina, Semicond. Sci. Technol. **23**, 075001 (2008).
[8] M. Casalino, G. Coppola, M. Gioffrè, M. Iodice, L. Moretti, I. Rendina, and L. Sirleto, J. Lightwave Technol. **28**, 3266 (2010).
[9] C. Scales, I. Breukelaar, R. Charbonneau, and P. Berini, J. Lightwave Technol. **29**, 1852 (2011).
[10] A. R. Zali, M. K. Moravvej-Farshi, and G. Abaeiani, Opt. Lett. **37**, 4925 (2012).
[11] I. Goykhman, U. Sassi, B. Desiatov, N. Mazurski, S. Milana, D. de Fazio, A. Eiden, J. Khurgin, J. Shappir, U. Levy, and A. C. Ferrari, Nano Lett. **16**, 3005 (2016).
[12] C. Scales and P. Berini, IEEE J. Quant. Electron. **46**, 633 (2010).
[13] S. Zhu, M. Yu, G. Lo, and D. Kwong, Appl. Phys. Lett. **92**, 81103 (2008).
[14] M. Hosseinifar, V. Ahmadi, and M. Ebnali-Heidari, IEEE Photon. Technol. Lett. **28**, 1363 (2016).
[15] M. Casalino, G. Coppola, M. Iodice, I. Rendina, and L. Sirleto, Opt. Express **20**, 12599 (2012).
[16] A. Taghizadeh, J. Mørk, and I. S. Chung, Appl. Phys. Lett. **107**, 181107 (2015).
[17] C. F. Mateus, M. C. Huang, Y. Deng, A. R. Neureuther, and C. J. Chang-Hasnain, IEEE Photon. Technol. Lett. **16**, 518 (2004).
[18] R. Orta, A. Tibaldi, and P. Debernardi, IEEE J. Quant. Electron. **52**, 1 (2016).
[19] A. Taghizadeh, J. Mork, and I.-S. Chung, Opt. Express **23**, 14913 (2015).
[20] A. Taghizadeh, G. C. Park, J. Mørk, and I.-S. Chung, Opt. Express **22**, 21175 (2014).
[21] A. Taghizadeh and I.-S. Chung, Sci. Rep. **7**, 2123 (2017).
[22] K. Ikeda, K. Takeuchi, K. Takayose, I.-S. Chung, J. Mørk, and H. Kawaguchi, Appl. Opt. **52**, 1049 (2013).
[23] R. H. Fowler, Phys. Rev. **38**, 45 (1931).
[24] P. Berini, A. Olivieri, and C. Chen, Nanotechnology **23**, 444011 (2012).
[25] A. Akbari, A. Olivieri, and P. Berini, IEEE J. Sel. Top. Quantum Electron. **19**, 4600209 (2013).
[26] S. Zhu, G. Lo, and D. Kwong, Opt. Express **19**, 15843 (2011).
[27] J. R. Piper, V. Liu, and S. Fan, Appl. Phys. Lett. **104**, 251110 (2014).
[28] B. C. Sturmberg, T. K. Chong, D.-Y. Choi, T. P. White, L. C. Botten, K. B. Dossou, C. G. Poulton, K. R. Catchpole, R. C. McPhedran, and C. M. de Sterke, Optica **3**, 556 (2016).
[29] Y. Chong, L. Ge, H. Cao, and A. D. Stone, Phys. Rev. Lett. **105**, 053901 (2010).
[30] W. Wan, Y. Chong, L. Ge, H. Noh, A. D. Stone, and H. Cao, Science **331**, 889 (2011).
[31] A. Yariv, IEEE Photon. Technol. Lett. **14**, 483 (2002).
[32] K. Kishino, M. S. Unlu, J.-I. Chyi, J. Reed, L. Arsenault, and H. Morkoc, IEEE J. Quant. Electron. **27**, 2025 (1991).
[33] H. Zhou, B. Zhen, C. W. Hsu, O. D. Miller, S. G. Johnson, J. D. Joannopoulos, and M. Soljačić, Optica **3**, 1079 (2016).
[34] A. Taghizadeh, J. Mørk, and I.-S. Chung, J. Lightwave Technol. **34**, 4240 (2016).
[35] A. Taghizadeh and I.-S. Chung, Appl. Phys. Lett. **111**, 031114 (2017).
[36] M. Moharam, T. Gaylord, E. B. Grann, and D. A. Pommet, J. Opt. Soc. Am. **12**, 1068 (1995).
[37] L. Li, J. Opt. Soc. Am. A **13**, 1870 (1996).
[38] R. Vardanyan, V. Dallakyan, U. Kerst, and C. Boit, J. Contemp. Phys. **47**, 73 (2012).
[39] J. A. Giese, J. W. Yoon, B. R. Wenner, J. W. Allen, M. S. Allen, and R. Magnusson, Opt. Lett. **39**, 486 (2014).
[40] S. Fan, W. Suh, and J. Joannopoulos, J. Opt. Soc. Am. A **20**, 569 (2003).